Earthquakes and Structures, *Vol. 7, No. 6 (2014) 1001-1024*
DOI: http://dx.doi.org/10.12989/eas.2014.7.6.1001

Rocking behavior of bridge piers with spread footings under cyclic loading and earthquake excitation

Hsiao-Hui Hung*[1], Kuang-Yen Liu[1a] and Kuo-Chun Chang[1,2b]

[1]National Center for Research on Earthquake Engineering, Taipei, Taiwan
[2]Department of Civil Engineering, National Taiwan University, Taipei, Taiwan

(Received February 19, 2014, Revised August 10, 2014, Accepted August 22, 2014)

Abstract. The size of spread footings was found to be unnecessarily large from some actual engineering practices constructed in Taiwan, due to the strict design provisions related to footing uplift. According to the earlier design code in Taiwan, the footing uplift involving separation of footing from subsoil was permitted to be only up to one-half of the foundation base area, as the applied moment reaches the value of plastic moment capacity of the column. The reason for this provision was that rocking of spread footings was not a favorable mechanism. However, recent research has indicated that rocking itself may not be detrimental to seismic performance and, in fact, may act as a form of seismic isolation mechanism. In order to clarify the effects of the relative strength between column and foundation on the rocking behavior of a column, six circular reinforced concrete (RC) columns were designed and constructed and a series of rocking experiments were performed. During the tests, columns rested on a rubber pad to allow rocking to take place. Experimental variables included the dimensions of the footings, the strength and ductility capacity of the columns and the intensity of the applied earthquake. Experimental data for the six circular RC columns subjected to quasi-static and pseudo-dynamic loading are presented. Results of each cyclic loading test are compared against the benchmark test with fixed-base conditions. By comparing the experimental responses of the specimens with different design details, a key parameter of rocking behavior related to footing size and column strength is identified. For a properly designed column with the parameter higher than 1, the beneficial effects of rocking in reducing ductility and the strength demand of columns is verified.

Keywords: rocking; spread footing foundation; cyclic loading test; pseudo-dynamic test; bridge piers

1. Introduction

After the Chi-Chi earthquake, Taiwan increased the design values for earthquake intensity in some areas, resulting in the commencement of retrofitting of several bridges to satisfy the new code requirements. The works on these bridges required an increase in the plastic moment capacity of the columns, which ultimately increased demand on the foundation, based on capacity design. This has resulted in the very conservative and uneconomical design of large spread footings. This

*Corresponding author, Research Fellow, E-mail: hhung@narlabs.org.tw
[a]Associate Researcher, E-mail: kyliu@narlabs.org.tw
[b]Professor, E-mail: ciekuo@ntu.edu.tw

http://www.techno-press.org/?journal=eas&subpage=7 ISSN: 2092-7614 (Print), 2092-7622 (Online)

is because, in the current design philosophy, earthquake energy dissipation should rely on the plastic deformation of the column. Before a plastic hinge is formed at the column, the footing has to remain in its elastic state without any uplift. The rocking mode of a spread footing foundation, which allows the foundation to separate from the base soil, is still not considered a favorable design choice.

It was observed that rocking modes were not considered in the design of most structures in the 20th century, despite evidence of rocking and its benefits in historical data during the world's strongest earthquakes. Housner (1963) was the first to raise this issue when he noticed the survival of some apparently unstable structures in the Chilean earthquake in 1960 due to rocking action. A similar phenomenon was also observed in earthquakes in Arvin–Tehachapi in 1952, Alaska in 1964, California in 1979 (Psycharis 1982) and other earthquakes in Japan (Kawashima and Nagai 2006). Most recent evidence came from Apostolou *et al.* (2007) who noted rocking action in the Kocaeli and Athens earthquakes in 1999.

Rocking of the spread footings of the bridge pier from the underlying soil induces nonlinear behavior in the foundation, which comes from the uplift or separation of the spread footings and energy dissipation deriving from the inelastic properties of the soil. These two actions can reduce the demands on bridge structures, thereby decreasing the plastic deformation that occurs in the plastic zone. In other words, a smaller foundation size that allows the structure to rock might be more advantageous than a large foundation size that fixes the structure to the ground. Besides, since spread footing foundations solely rely on the weight of the structure to resist external loads, unless the foundation is very massive, it is reasonable to expect that uplifting of the foundation would still occur during strong earthquakes. This is regardless of whether it is considered, as can be observed in past earthquakes. For these reasons, it is reasonable to tolerate a certain amount of uplift in the spread footing foundation in the design of a bridge, especially in the retrofitting of the foundation. In fact, foundation rocking has been conditionally accepted by some retrofitting guidelines or manuals, including the FEMA (1997) for buildings, and the FHWA (2006) for bridges. In Taiwan, the stability check of a spread footing in the design code (MOTC 2008) was also revised recently to allow a certain amount of foundation uplift to occur in the ultimate state.

Despite the past research on the benefits of rocking, current mainstream design philosophy still does not see rocking of the foundation as a favorable choice in general and it is not taken into account in analysis, especially for new bridge designs. For instance, although AASHTO (2009) provides a recommendation for the design procedure of rocking bridge piers and a method to predict the rocking displacement, the adoption of the rocking mechanism requires the owner's approval. In the loadings code of New Zealand, the energy dissipation through rocking is also only conditionally allowed if a special study is performed (Kelly 2009). This is probably due to the lacking of important experimental databases and of robust nonlinear analytical models which is capable of extensively reproducing coupled material and geometrical nonlinearities behavior involved in the foundation rocking. As a result, the possible disadvantages that might be brought by rocking, such as the increase in displacement demand at the deck level and settlement in the foundation are difficult to be predicted precisely. Moreover, in the strength design approach which is still widely used in many countries, neglecting the effects of rocking would simply overestimate the seismic forces applied to the structures and lean towards the conservative side. Thus, many design codes would rather choose to prevent rocking.

However, with increasing awareness of performance-based design, a more precise prediction of how the structure would behave under seismic loading becomes crucial. This includes a reasonable prediction of the lateral displacements in the column top, prediction of the amount of rocking and structural deformation, by realistically considering interaction between the foundation, the column and the soil. Additionally, as mentioned earlier, some uplift on the edge of the foundation is highly likely to occur under severe earthquake conditions. The evidence of footing uplift during past earthquakes seems to indicate that, even though the possible benefits gained from foundation rocking were not taken into account in the design phase, rocking has occurred in the past during severe earthquakes. The insistence on neglecting the effects of rocking sometimes underestimates the disadvantages that may be brought by rocking, such as large lateral displacements of the deck and permanent settlement in the soil. This means designs neglecting the effects of foundation rocking would not always be on the conservative side. In this regard, the realistic approach, where the effects of rocking are considered, including the interaction between the foundation, the column and the soil, has gradually become an important issue in the structural design of bridges.

The effectiveness of the rocking mechanism to mitigate the effects of earthquakes on structures has been identified in many previous studies since the pioneering work performed by Housner (1963). Over the following decades, several other articles have been published on the study of rocking behavior. These studies have indicated the benefits of the rocking mechanism in dissipating energy. However, most of these studies have focused on rigid block structures (Aslam *et al.* 1980; Yim *et al.* 1980; Tso and Wong 1989; Yang *et al.* 2000; Zhang and Makris 2001) or rigid structures (Apostolou *et al.* 2007; Palmeri and Makris 2008). Yim and Chopra (1984) and Chopra and Yim (1985) were among the first to develop a better understanding of the effects of transient foundation uplift on the response of flexible and elastic structures. It should be noted that most of these earlier studies on the rocking mechanism were performed using an analytical approach and relatively few experimental studies, especially in the case of large-scale tests, were carried out. With the current advances in experimental technique, rocking experiments have become the focus of several studies recently. Simultaneously, more elaborate analytical models have been proposed to simulate these experiments.

The experimental studies can generally be categorized into two groups. The first group consists of studies conducted mainly from a geotechnical point of view that tend to concentrate on the coupling effects of foundation uplift and soil nonlinearity that could result in the permanent deformation of the underlying soil. The second group consists of studies conducted mainly from a structural perspective and focused on the nonlinear behavior of columns as a result of foundation rocking. For experiments of the first group, test foundation models were placed mostly on real soil in a soil container. Due to the size limit of soil containers, most of these test models were small and were performed in a geotechnical centrifuge to eliminate the size effect and to retain the proper prototype soil stresses. For instance, Gajan *et al.* (2005) and Gajan and Kutter (2008) performed several series of tests on a large centrifuge at 20 g centrifugal acceleration to simulate the behavior of a prototype shear wall footing using a 1/20-scale model. To understand the rocking behavior of bridges on shallow foundations under nonlinear moment, shear, and vertical loading, Ugalde *et al.* (2007, 2010) also performed several centrifugal tests on 1/42.9-scale single-column models on shallow foundations at 42.9 g centrifugal acceleration at UC Davis. Based on these experiments, two advanced analytical models were proposed: a beam-on-nonlinear-Winkler-foundation model (BNWF) and a contact interface model (CIM) (Harden *et al.* 2005; Kutter *et al.* 2005; Gajan *et al.* 2007). Very recently, Deng *et al.* (2012) performed several centrifugal model tests for both single-column models and full bridge system models at UC Davis at 40 g and 49 g centrifugal accelerations. These experiments concluded that tipping instability of a bridge was unlikely if the foundations were property sized. Deng and Kutter (2012) also performed another series of centrifugal model test at 49 g centrifugal acceleration to explore the behavior of rocking in shallow foundations embedded in dry sand and found that if the factor of safety for vertical bearing was reasonably large, the settlement was shown to be small. Other experimental tests were performed on real soil but at low normal stresses (model tests at 1 g) including those that were performed more than 30 years ago in New Zealand (Wiessing 1979; Taylor *et al.* 1981) and the recent shaking table tests performed by Shirato *et al.* (2008) at the Public Works Research Institute in Japan. The experiment in Japan was conducted to investigate the model of a shallow pier foundation resting at the surface of a laminar box filled with dry sand excited using real earthquake data at various levels of amplitude. Based on this experiment, Paolucci *et al.* (2008) proposed a simplified elasto-plastic macro-element model to simulate the behavior of shallow foundations during an earthquake. Cremer *et al.* (2001) also proposed a non-linear soil-structure interaction macro-element for shallow foundation which can reproduce the material nonlinearities of soil and geometric nonlinearities due to uplift. The relevance of the model was verified through the comparison with FE modeling. Grange *et al.* (2009a) proposed a 3D nonlinear interface element also based on the macro element concept to simulate 3D soil structure interaction considering plastic and uplift. Afterward a similar model which can simulate dynamic soil-structure interaction was also proposed by Grange *et al.* (2009b). The performance of both models was validated using experimental results which were performed earlier. Using this developed macro-element, Grange *et al.* (2011) also performed a parametric study to show the influence of foundation uplift and soil plasticity on the nonlinear behavior of a reinforced concrete viaduct.

On the other hand, the second group that concentrated on pier behavior mostly performed their tests on a shaking table and adopted a neoprene pad as a substitute for the soil, like that used in the shaking table tests of small-scale steel columns performed by Sakellaraki *et al.* (2005) and in the moderate-scale reinforced concrete (RC) bridge column tests performed by Espinoza and Mahin (2006). The columns in both these experimental studies were designed to remain in their elastic response behavior when excited by the input of a ground motion, thus removing the need to consider the plastic deformation of a column at the plastic hinge. Both tests showed that even though the level of excitation would have severely damaged a fixed-base column, the test rocking columns were not damaged and had re-centered following the shaking.

All of these previous studies have recognized the beneficial effects of rocking. However, even though some of the analytical models have the ability to simulate the coupling effect between non-linearity in the soil and in the bridge piers and their results have revealed advantages towards allowing rocking mechanisms in the design to reduce plastic deformation, such as those noted by Kawashima and Nagai (2006) and Grange *et al.* (2011), few of experimental studies have considered the coupling effect of the material nonlinearity that is involved with column plastic hinging and the geometrical nonlinearity due to foundation uplift. The analytical approaches still need more experimental evidence to support their results. In addition, the relevant research is not sufficiently comprehensive to provide confidence to extensively revise the design code. In order to obtain good references for future seismic evaluations and design codes, more experimental data are required. A preliminary experiment was performed by Hung *et al.* (2011) to investigate the rocking behavior of both lightly transverse-reinforced columns and retrofitted columns in order to clarify the necessity of widening and strengthening of the foundations to limit the rocking mechanism of spread footing for retrofitting work. From this experiment, an isolation effect of a rocking spread footing foundation was observed. However, the focus of the previous study was on the existing bridge columns for which retrofit were required and the number of test specimens in the previous experiment was also not enough to have a design covering all the range of interest.

Therefore, in this study, six RC columns with differing strengths, ductility capacities and footing dimensions were designed and constructed. A series of pseudo-dynamic and cyclic loading tests were conducted on these specimens. The focus of this experiment was to investigate the interactive relationship between the strength capacity of the column and the foundation, as well as the effects of this interactive relationship on the overall rocking behavior of columns with spread footings.

2. Theoretical calculations for the rocking mechanism

In order to make sure that the experiment successfully investigates the coupling effects of material nonlinearity in column hinging and the geometrical nonlinearity in footing uplift, before the experimental specimens were designed and constructed, the basic theory for the rocking mechanism studied in the previous paper (Hung *et al.* 2011) will be summarized here.

For a column with a spread footing standing on soil, the footing would lift off the ground once its moment of resistance provided by gravity has been overcome. Thus, the moment at the base of the foundation would be limited to the value required to induce uplift against the gravitational restraining forces. By assuming that the underlying soil is a perfect plastic material with an ultimate stress of q_y, according to force equilibrium, the limit of the moment that can be resisted by this rigid rectangular foundation, noted by M_2, is calculated by (FHWA, 2006):

$$M_2 = \frac{BW_T}{2}\left(1 - \frac{q}{q_y}\right), \tag{1}$$

where B is the width of the footing in the direction of the bending moment, W_T is the total axial load applied to the foundation base, q is the contact stress under the foundation equal to $W_T/(B \times L)$, where L denotes the length of the foundation. This limit also implies that if the footing of a column was allowed to rock with the uplift, the shear force and the bending moment that the column has to sustain would also have an upper limit value. The upper limit of the shear force V_{2c} and bending moment M_{2c} at the column base can be derived from the value of M_2, with:

$$V_{2c} = \frac{M_2}{H} = \frac{BW_T}{2H}\left(1 - \frac{q}{q_y}\right) \text{ and} \tag{2}$$

$$M_{2c} = V_{2c}(H - h) = \frac{BW_T}{2H}(H - h)\left(1 - \frac{q}{q_y}\right) \tag{3}$$

where H is the distance between the location where the lateral force applies and the foundation base, and h is the height of the foundation.

Furthermore, if it is assumed that the ultimate stress of q_y is far larger than q, which is the case for the majority of spread footings that are supported by stiff soil, then the value of q/q_y in Eqs. (2) and (3) approaches zero and the limit of the shear force and the bending moment that the column is able to sustain depends only on the footing size and the total vertical force of gravity. Since M_{2c} is the upper limit of the bending moment that the column has to sustain, it is obvious that the ratio of the strength capacity of the column, M_y, to the upper limit moment, M_{2c}, calculated in Eq. (3), is the key parameter for the seismic performance of the column with a spread footing. It is expected that if the bending moment capacity of the column M_y is larger than the limit M_{2c}, the response behavior of the column-footing system would be governed by rocking of the footing and plastic deformation would not occur at the column base. On the other hand, if the bending moment capacity of the column M_y was lower than the bending moment M_{0c} at the column base that is required to induce uplift, i.e.,

$$M_{0c} = \frac{BW_T}{6H}\left(H - h\right) \tag{4}$$

the rocking mechanism would not be triggered and the column with spread footings would respond much the same as a column with a fixed base. However, if the bending moment capacity of a column was between M_{2c} and M_{0c}, it would be highly likely that both the material nonlinearity involved with column plastic hinging and the geometrical nonlinearity due to footing uplift would help to dissipate some energy during strong earthquakes. Therefore, the upper limit value, M_{2c}, which is actually due to the capacity of the spread footing, could also be referred to as the maximum demand of the columns.

3. Experimental program

Based on the theoretical calculations in the previous section, columns with two types of foundation size and three types of base design were designed to cover the ratio of the column's capacity to its maximum demand M_y/M_{2c} in varying ranges. A total of six specimens were tested in the current study. A short summary of the experiments is provided here, including the experimental set-up, the recording system and the sequence of the tests.

3.1 Test specimens

Six RC columns with two types of foundation size and three types of column base design were designed and constructed. As shown in Fig. 1, these circular RC columns were all 50 cm in diameter with a clear height of 2.5 m and a footing height of 50 cm. Their footing sizes were either B = 140 cm or B = 170 cm. Thus, according to Eq. (3), the corresponding upper limit of the bending moment for the specimens with the smaller footing (B = 140 cm, W_T = 574 kN) was M_{2c} = 334.8 kNm. For the specimens with the larger footing (B = 170 cm, W_T = 585 kN), the corresponding upper limit was M_{2c} = 414.4 kNm. In order to compare the rocking performance of the specimens with different ratios of the moment capacity of the column to the upper limit moment, M_{2c}, these test columns were reinforced with three different designs. One specimen with 12-D19 (steel ratio = 1.75%) main reinforcement was transversely reinforced with D13 perimeter hoops spaced at 9 cm (volumetric confinement ratio ρ_s = 0.012), representing a case with sufficient transverse reinforcements. The other two with 18-D19 (steel ratio = 2.63%) main reinforcement were transversely reinforced with D13 perimeter hoops spaced at 9 cm and 18 cm, respectively. The latter specimen with the 18 cm spacing was designed to represent a column with an insufficient volumetric confinement ratio (ρ_s = 0.006) in order to investigate the effects of ductility capacity on a column's rocking behavior. The nominal material properties for these specimens are as follows: concrete compressive strength $f_c^{'}$ = 27.5 MPa, yield strength of main reinforcements F_y = 412.0 MPa, and yield strength of the transverse reinforcements F_{yh} = 274.7 MPa.

By varying the combinations of the different footing dimensions and design details, a total of six test columns were designed and named CD40FS-R, CB40FS-R, CD30FS-R, CD40FB-R, CD30FB-R and CD30FB-F, respectively. These are plotted in Fig. 1 and listed in Table 1. The letters "CD" and "CB" denote columns that were transversely reinforced with perimeter hoops

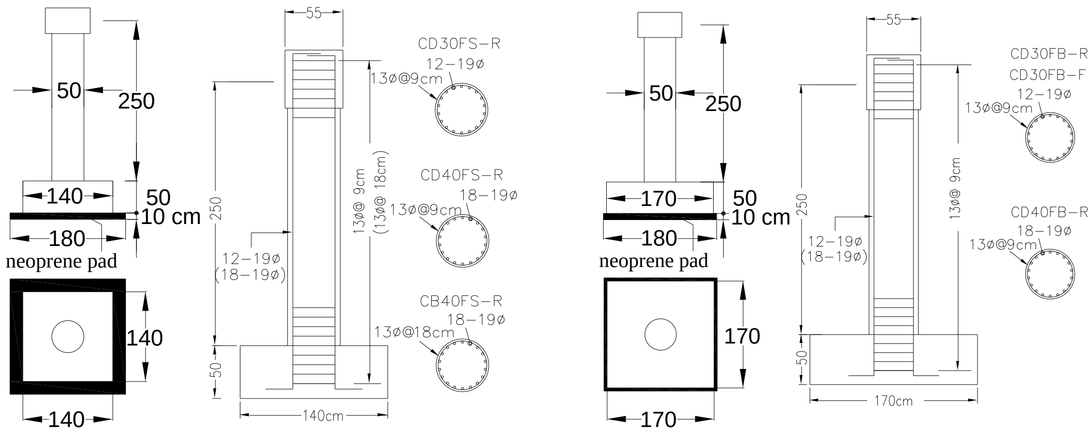

(a) B = 140 cm (b) B = 170 cm

Fig. 1 As-built details of the model columns (unit: cm)

Table 1 Design details and the experimental test schedule

Test Specimens	Design details	Base condition	Tests
CD40FS-R	Footing: 140×140 cm 18-D19 with stirrup: D13 @ 9 cm	Rocking base	pseudo-dynamic test (TH1,TH2) cyclic loading test
		Fixed base	cyclic loading test
CD30FS-R	Footing: 140×140 cm 12-D19 with stirrup: D13 @ 9 cm	Rocking base	pseudo-dynamic test (TH1,TH2) cyclic loading test
CD40FB-R	Footing: 170×170 cm 18-D19 with stirrup: D13 @ 9 cm	Rocking base	pseudo-dynamic test (TH1,TH2) cyclic loading test
CD30FB-R	Footing: 170×170 cm 12-D19 with stirrup: D13 @ 9 cm	Rocking base	pseudo-dynamic test (TH1,TH2) cyclic loading test
CB40FS-R	Footing: 140×140 cm 18-D19 with stirrup: D13 @ 18 cm	Rocking base Fixed base	cyclic loading test cyclic loading test
CD30FB-F	Footing: 170×170 cm 12-D19 with stirrup: D13 @ 9 cm	Fixed base	cyclic loading test

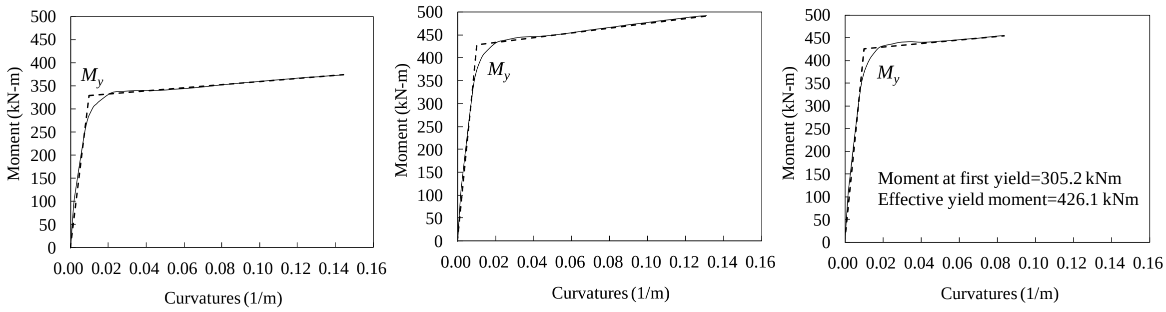

(a) Specimen CD30xx-x (b) Specimen CD40xx-x (c) Specimen CB40xx-x

Fig. 2 Moment–curvature curves of the model columns

spaced 9 cm and 18 cm, respectively. The numbers “40” and “30” denote cases with 18-D19 and 12-D19 main reinforcements, respectively. The letters “FS” and “FB” denote cases with the smaller footing (B = 140 cm) and the larger footing (B = 170 cm), respectively. The letters “R” and “F” represent the rocking base condition and fixed-base condition, respectively.

Based on the nominal material properties, the moment capacities of these specimens were also calculated from the moment–curvature analysis. The calculated moment–curvature curves are shown in Fig. 2. In this paper, the effective yield moments M_y are used to represent the moment capacity of the column. The effective yield moment is the turning point of the idealized moment-curvature curve which is bilinearized as shown in the dotted line in Fig. 2. The idealized bilinear curve can be obtained by making the elastic portion of the curve pass through the point as the first reinforcing bar yields and adjusting the post slope of the curve to make the areas under the actual and the idealized moment-curvature curves equal. As can be seen, the effective yield moments of specimens labeled CD30, CD40 and CB40 were 329.0 kNm, 428.3 kNm and 426.1 kNm, respectively. Therefore, the ratios of the moment capacity of the column, M_y, to the upper limit moment, M_{2c}, for specimens CD40FS-R, CD40FB-R, CD30FS-R and CD30FB-R were 1.28, 1.03, 0.98 and 0.79, respectively. Specimen CB40FS-R had the same ratio as CD40FS-R. Obviously, the ratios for these specimens cover the range of interest for this experiment i.e., from 0.79 to 1.28.

3.2 Test setups

To clarify the difference in the response behavior between columns with a rocking-base condition and those with a fixed-base condition, tests were conducted both with and without a footing uplift restraint. Fig. 3 illustrates the test setup. In the case where footing uplift was restrained, four tie-down rods were placed through the footing and anchored into the strong floor of the laboratory to restrain the rocking mode of the foundation (Fig. 3(b)). In the case where the rocking mechanism was considered (Fig. 3(a)), the square footings rested on a 10 cm thick neoprene pad (Duro-60), simulating a spread footing foundation in a stiff soil. The size of the neoprene pad was 180×180 cm. During the test, the lateral deformation of the neoprene pad was restrained. In addition, a special apparatus with rolling balls was installed on each side of the foundation to prevent torsion of the test columns but allowing uplift of the footing.

During the test, a constant axial load of 539 kN, which was around $0.10A_gf_c'$, was applied to the test column through a tap beam using two vertical actuators to simulate the tributary dead load of

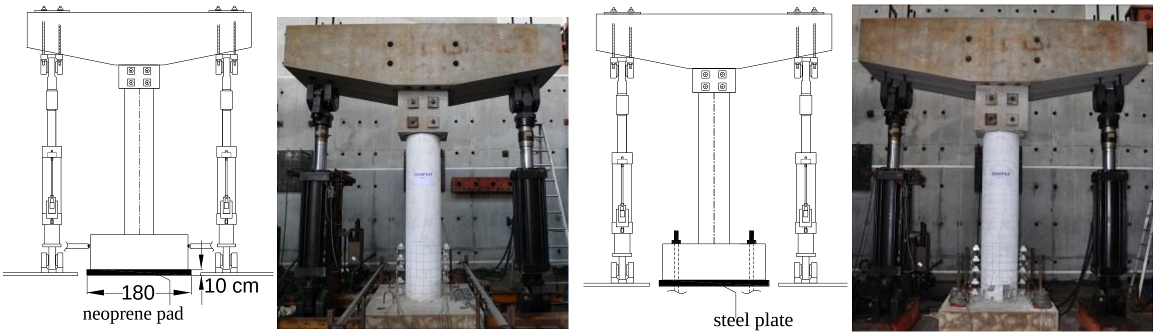

(a) Rocking base (b) Fixed base

Fig. 3 Test setups

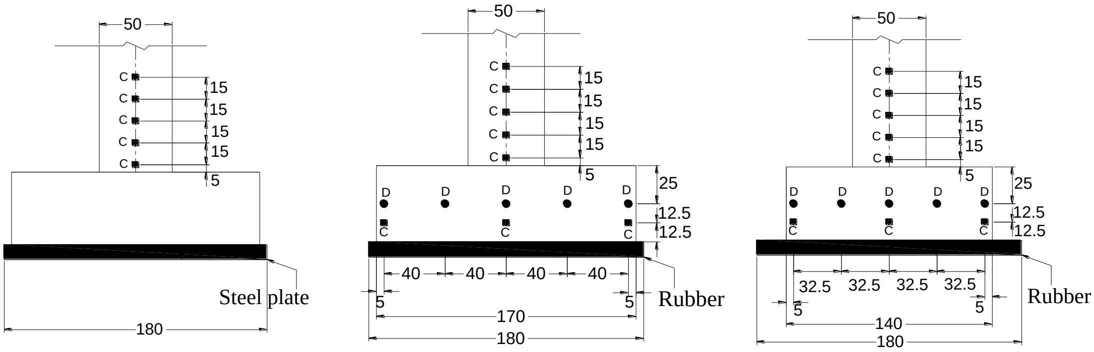

(a) fixed base (b) B=170 cm (c) B=140 cm

Fig. 4 Layout of instrumentation (unit:cm)

the deck, where A_g represents the gross cross-sectional area of the column. In addition, one horizontal actuator was used to apply the lateral force to the column's top to simulate seismic loading. The location of the application force was 2.5 m above the top of the footing, and 3 m above the footing base. Under the excitation of the loading, the uplift displacements and rotations of the foundation were monitored by ten string pots and ten tiltmeters mounted on two sides of the foundation. Curvatures and rotations within the region of the plastic hinge in the columns were also measured using ten tiltmeters in two lines mounted on each side of the columns along the neutral axis in the potential plastic hinge zone. The instrumentation layouts for the fixed base case and the rocking base cases with foundation B=170 cm and B=140 cm are shown in Figures 4(a), (b) and (c), respectively, where symbol C denotes the tiltmeter to measure rotation, and symbol D denotes the string pot to measure uplift displacement.

3.3 Test schedule

The test schedule is listed in Table 1 and includes the pseudo-dynamic loading test and the quasi-static cyclic loading test. The input ground motions for the pseudo-dynamic test are shown in Fig. 5 and the lateral loading sequence for the cyclic loading test is shown in Fig. 6. The input ground motions were two different artificial earthquake accelerations which were compatible to the seismic design code for highway bridges in Taiwan (MOTC 2008). One was a medium earthquake acceleration (TH1) whilst the other was a design earthquake acceleration (TH2) for Nantou Pouli, a region of high seismicity in Taiwan. As shown in Figs. 5 and 6, the peak ground motions for TH1 and TH2 were 100 cm/s^2 and 326 cm/s^2, respectively, and the cyclic tests were performed under displacement control to a drift ratio of 7% (17.5 cm). For specimens CD40FS-R, CD30FS-R, CD40FB-R and CD30FB-R, the columns were first sequentially tested by two pseudo-dynamic loadings, i.e., TH1 and TH2, under the rocking base condition. These four specimens and another specimen, CB40FS-R, were then subjected to a cyclic loading test. Since no physical damage was observed in specimens CD40FS-R and CB40FS-R at the completion of the rocking base testing, the same specimens were later fixed to the strong floor and tested by another cyclic loading test, acting as benchmark tests for the fixed-base condition. Specimen CD30FB-F, which has the same design as CD30FB-R, also underwent a cyclic loading test under the fixed-base condition to provide a benchmark for columns with 12-D19 main reinforcements.

For a rocking-base column, the lateral displacement at the column top was one of the major concerns for its structural design. The lateral displacement at the top of column cannot be too large so as to jeopardize the stability of the column and affect the functionality of the bridge. Therefore, the purpose of the pseudo-dynamic test was to estimate the lateral displacement demand due to the rocking effect under earthquake excitations with different levels of intensity. In this study, a single-degree-of-freedom system was assumed to establish the equation of motion for each pseudo-dynamic test. During the test, the reaction force that included the effect of inelastic forces due to material nonlinearity of the column and geometric nonlinearity of foundation uplift was

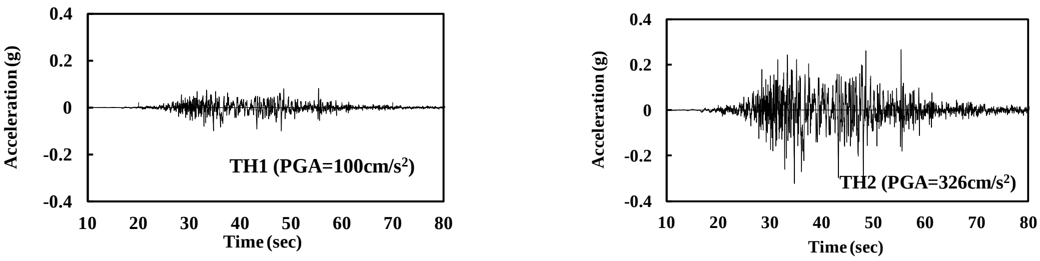

(a) TH1 (b) TH2

Fig. 5 Input ground motions for the pseudo-dynamic tests

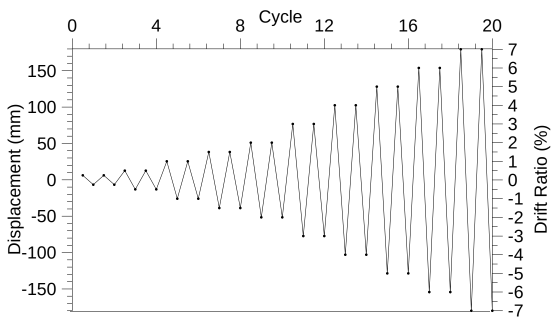

Fig. 6 Loading sequence for the cyclic loading test

measured. Based on this measurement and the hypothetical values for mass and damping that were prescribed before the tests, the inertial force that the model would have been exposed to during the actual earthquake was inferred and the lateral displacement was computed for the next step. The actuator was then commanded to achieve this target lateral displacement. The overall procedure was repeated until the end of the excitation time history. In the current pseudo-dynamic test, the system was assumed to have a mass of 55,000 kg to simulate the tributary dead load of the deck weight and a damping ratio of five percent. Based on the assumption of the tributary dead load, the structural period of the test column under fixed-base condition is 0.36 sec, which was obtained from modal analysis. On the other hand, the purpose of the quasi-static cyclic loading test was to investigate the effect of foundation size on the overall capacity of the column which was allowed to rock.

4. Test results and discussion

The results obtained from the experiments are summarized as follows.

4.1 Pseudo-dynamic tests of TH1

As mentioned previously, specimens CD40FS-R, CD30FS-R, CD40FB-R and CD30FB-R were first supported on a neoprene pad without any uplift restraint and were subjected to the pseudo-dynamic test of TH1. The hysteretic responses of these tests are plotted in Fig. 7. Fig. 7(a) shows the lateral load versus the lateral displacement curves for the system, and Fig. 7(b) shows the moment versus rotation curves at the column base. In these moment–rotation curves, the rotations

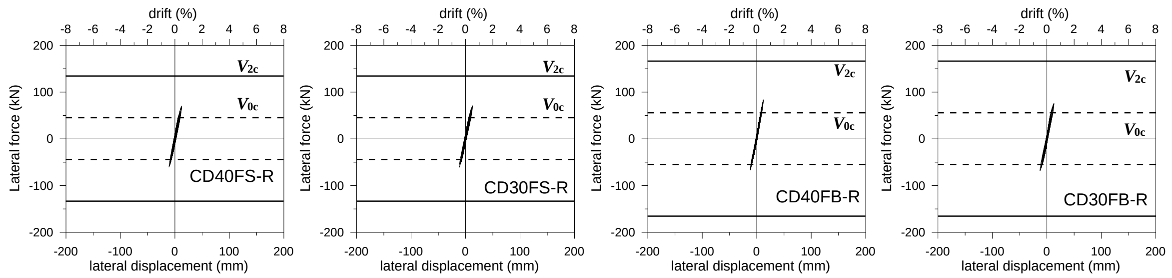

(a) force–displacement response

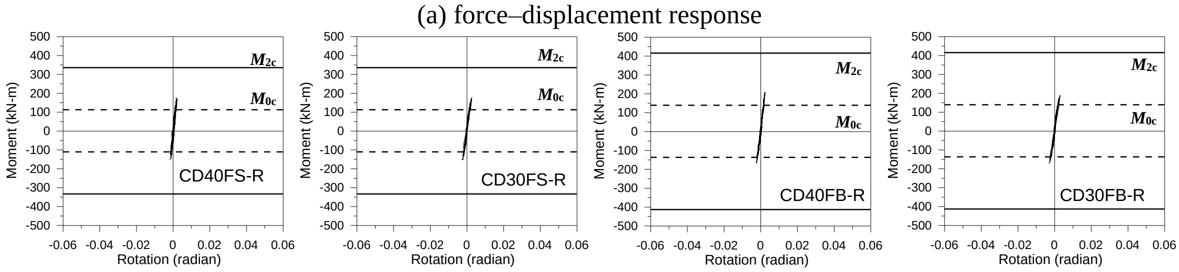

(b) moment–rotation response at the column base

Fig. 7 Experimental results for the pseudo-dynamic test of TH1

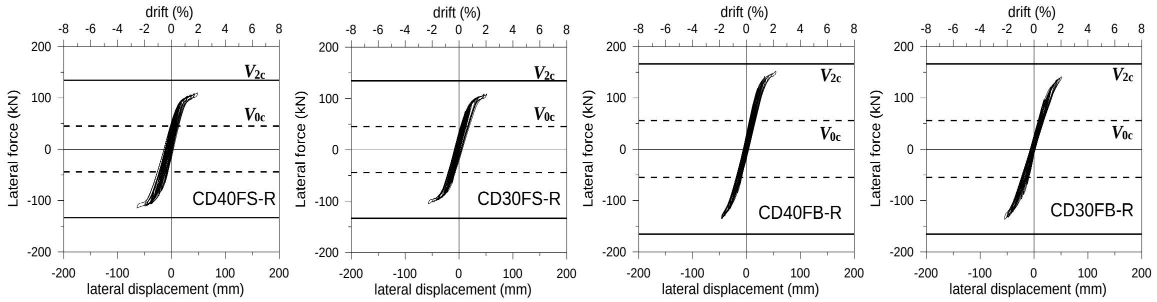

(a) force–displacement response

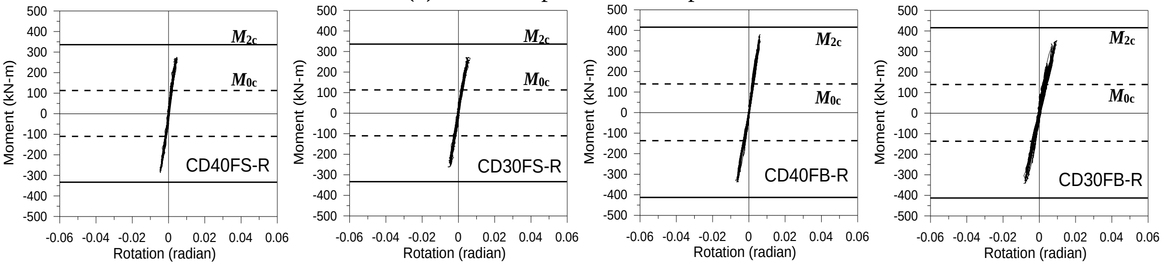

(b) moment–rotation response at the column base

Fig. 8 Experimental results for the pseudo-dynamic test of TH2

were obtained by taking the reading of the highest tiltmeter located at a height of 65 cm minus the reading of another tiltmeter mounted on the footing. Thus, the rotations in Fig. 7(b) come only from the elastic and plastic flexure of the columns, whereas the lateral displacements given in Fig. 7(a) come from the elastic and plastic flexure of the column plus the rocking of the footing.

Recalling from the theoretical calculations provided in Section 2, if the foundation of a column is allowed to rock with uplift and the yield stress of the underlying soils is assumed to be large enough that the soil will not yield during an earthquake, then the maximum upper limit of the shear force and bending moment that the column can resist can be calculated by Eqs. (2) and (3), respectively. Using these equations, the corresponding upper limit value of the shear force and the bending moment for the specimen with the larger foundation (B = 170 cm) were V_{2c} = 165.8 kN and M_{2c} = 414.4 kNm, respectively, while the specimens with the smaller footing (B = 140 cm), the values were V_{2c} = 133.9 kN and M_{2c} = 334.8 kNm, respectively. Eq. (4) gives the bending moment M_{0c} at the column base that is required to induce uplift, which can be obtained by dividing M_{2c} by 3. Correspondingly, the lateral force V_{0c} that is required to induce uplift can also be obtained by dividing V_{2c} by 3. In order to highlight the effect of these values on the pier behavior, three values of M_{2c}, M_{0c}, V_{2c} and V_{0c} were also presented graphically in Fig. 7.

From these figures, it is evident that under the excitation of TH1 acceleration, both the force–displacement curves and the moment–rotation curves remained almost linear. This is because the uplift of the footing was insignificant and that the plastic hinge had not formed while the columns experienced this minor earthquake. As can be seen in Fig. 7, the maximum lateral forces sustained by these columns are only slightly larger than V_{0c} and the maximum moments sustained by the specimens are still less than their corresponding effective yield moments. Another phenomenon that can be observed in Fig. 7 is that there were similar response behaviors in specimens with the same footing size. That is to say, specimens CD40FS-R and CD30FS-R had similar response behaviors, and specimens CD40FB-R and CD30FB-R also behaved similarly, even though their main reinforcement design details were different. An explanation could be that material nonlinearity was not developed in the column; therefore the influence of the reinforcement design details becomes insignificant. This observation also implies that the controlling parameter for the performance of these test columns subjected to such a minor earthquake was the dimension of the foundation and not the strength capacity of the column.

4.2 Pseudo-dynamic tests of TH2

After the pseudo-dynamic testing of TH1, the specimens CD40FS-R, CD30FS-R, CD40FB-R and CD30FB-R were subjected to pseudo-dynamic testing of TH2. The experimental results of the lateral force versus lateral displacement curves and the moment versus rotation curves are plotted in Figs. 8(a) and 8(b), respectively. By observing these figures, it was evident that subject to the design earthquake, the plastic deformation of the columns was still not noticeable. However, at the same time, some uplift already took place, since the lateral forces sustained by these columns were considerably larger than the value of V_{0c}, the shear force that can trigger the uplift. The uplift effect can also be easily identified by the lateral force–displacement curves, as they were no longer linear but rather showed a softer stiffness as the lateral displacement increased in a S-type form. This observation implies that some uplift occurred during the excitation of this design earthquake and resulted in some isolation effect.

Similar to the previous cases subjected to a frequent earthquake TH1, the response behaviors of CD40FS-R and CD30FS-R were similar, even though their main reinforcements were different. However, when testing specimens with the larger footing, the maximum values of the lateral force and the moment sustained by CD30FB-R was slightly smaller than those sustained by CD40FB-R. In addition, the area enclosed by the hysteresis loop of the moment–rotation curve for specimen CD30FB-R was slightly larger than that of CD40FB-R. This is because CD30FB-R had a moment strength less than that of CD40FB-R and had the design ratio of M_y / M_{2c} = 0.79, a value much lower than 1. As a result, CD30FB-R had already yielded a little before the rocking mechanism could fully control the response behavior. The same result can also be observed in the photograph of the test columns taken after each test, seen in Fig. 9. Some cracks can be observed on CD30FB-R in Fig. 9(d). However, there was no observable physical damage in the other three specimens.

To further investigate the rocking effect on the variation of structural period, the structural periods of these test specimens with respect to time were all calculated by performing short-time Fast Fourier Transform on the measured lateral displacements. To take specimen CD40FB as an example, the time history of the lateral displacements at the pier top and the variation of the calculated structural periods were both plotted in Figure 10, where Figs. (a) and (b) respectively represent the results under the pseudo-dynamic tests of TH1 and TH2. It shows that foundation uplift lengthened the structural period. In Fig. 10 (a) for the pseudo-dynamic tests of TH1, the structural period varied from 0.36 sec, which is the structural period of the test column under fixed base condition as has mentioned previously, to about 0.65 sec. As for the pseudo-dynamic tests of TH2 shown in Fig.(b), the structural period can be increased to around 1 sec, a value larger than that observed in Fig.(a). Since the rocking behaviour of the column under design earthquake was more significant than that in the case of a medium earthquake, the observed structural period for the column under design earthquake was larger than that under medium earthquake.

(a) CD40FS-R (b) CD30FS-R (c) CD40FB-R (d) CD30FB-R

Fig. 9 Photographs of the test columns after the pseudo-dynamic TH2 test

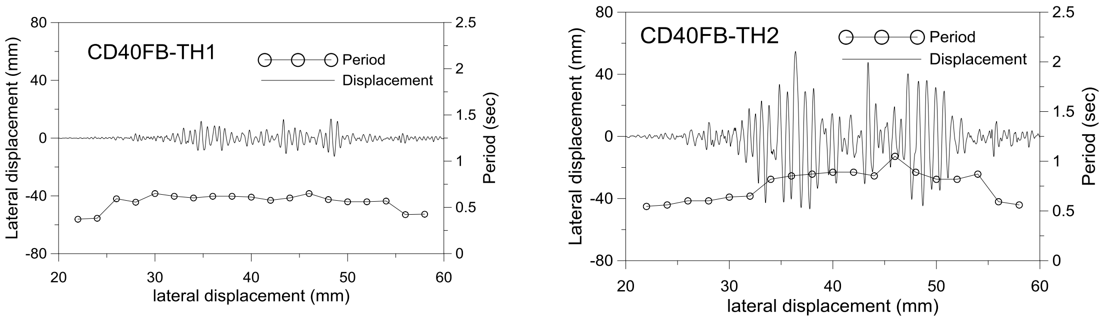

(a) TH1 (b) TH2

Fig. 10 Time history of the lateral displacement and structural period of specimen CD40FB under thepseudo-dynamic tests

4.3 Cyclic loading tests

For test columns CD40FS-R, CD30FS-R, CD40FB-R and CD30FB-R, after pseudo-dynamic tests were completed, cyclic loading tests were applied to these same test columns without uplift restraint. In order to investigate the influence of ductility on the performance of the column allowed to rock, test specimen CB40FS-R, which has a lower ductility, was also subjected to a cyclic loading test under the rocking base condition. For comparison, after these cyclic loading tests under rocking base condition were completed, because the observed damage on the specimens CD40FS-R, CB40FS-R was not obvious, another cyclic loading was applied to these two test columns again, but with uplift restraint to simulate fixed base cases, and these columns were renamed as CD40FS-F and CB40FS-F. In addition, a new specimen CD30FB-F was also tested by a cyclic loading test with uplift restraint.

These experimental results are plotted in Figs 11–22. Among these figures, Figures 11–14 show the experimental results of test specimens with 18-D19 main reinforcement and transversely reinforced with D13 hoops spaced at 9 cm (CD40xx.x). Figs 15–18 provide the results of specimens with 18-D19 main reinforcement and transversely reinforced with D13 perimeter hoops spaced at 18 cm (CB40xx.x). Figs. 19–22 demonstrate the results of test specimens with 12-D19 main reinforcement (CD30xx-x). Again, Figs. 11, 15 and 19 show the lateral force vs. lateral displacement curves, Figs. 12, 16 and 20 show the moment vs. rotation curves, Figs. 13, 17 and 21 show the vertical distribution of the curvature in the plastic hinge region for each test column, and Figs. 14, 18 and 22 show photographs of the specimens after the cyclic loading tests. The average curvature was obtained by taking the difference between the readings of two adjacent tiltmeters divided by the distance between them. For the sake of brevity, only the results for the push direction were plotted in these figures.

In these figures, the results for the fixed-base cases of CD40FS-F, CB40FS-F and CD30FB-F did not only signify the capacity of the columns with the same design details, but also represented cases with a very large footing size. For instance, CD40FS-F in Fig. 11 represented the case with the same design details as CD40FB-R and CD40FS-R but with a very large footing. By comparing the results of CD40FS-F, CD40FB-R and CD40FS-R in Figs. 11–13, it was noted that the rocking behavior was more pronounced as the dimension of footing decreased. In addition, the maximum lateral forces that the column sustained decreased with the decrease in footing size.

As shown in Figs. 11 and 12, these corresponding maximum values of shear forces and moments for CD40FB-R and CD40FS-R were respectively around V = 160 kN and 130 kN, and M = 400 kNm and 320 kNm, which were slightly lower than the upper limit values V_{2c} and M_{2c}. In addition, because the moments M_{2c} for CD40FB-R and CD40FS-R were less than the moment

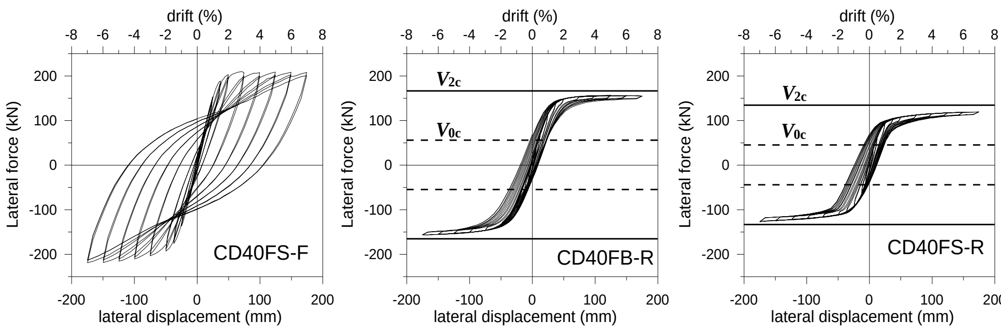

(a) CD40FS-F (b) CD40FB-R (c) CD40FS-R

Fig. 11 Lateral force–displacement curves of the cyclic loading tests of CD40xx-x

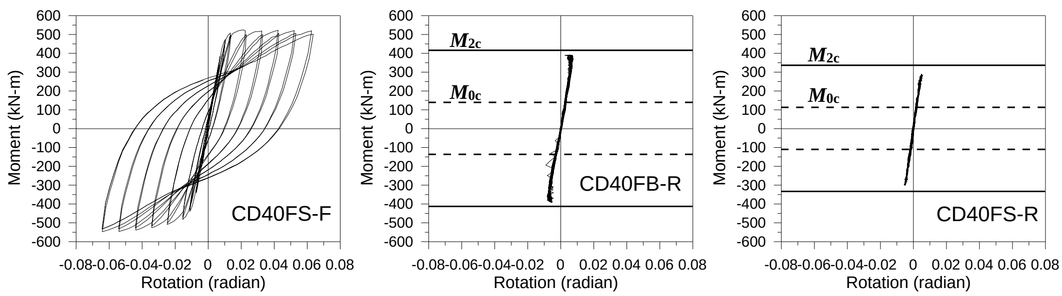

(a) CD40FS-F (b) CD40FB-R (c) CD40FS-R

Fig. 12 Moment–rotation curves of the cyclic loading tests of CD40xx-x

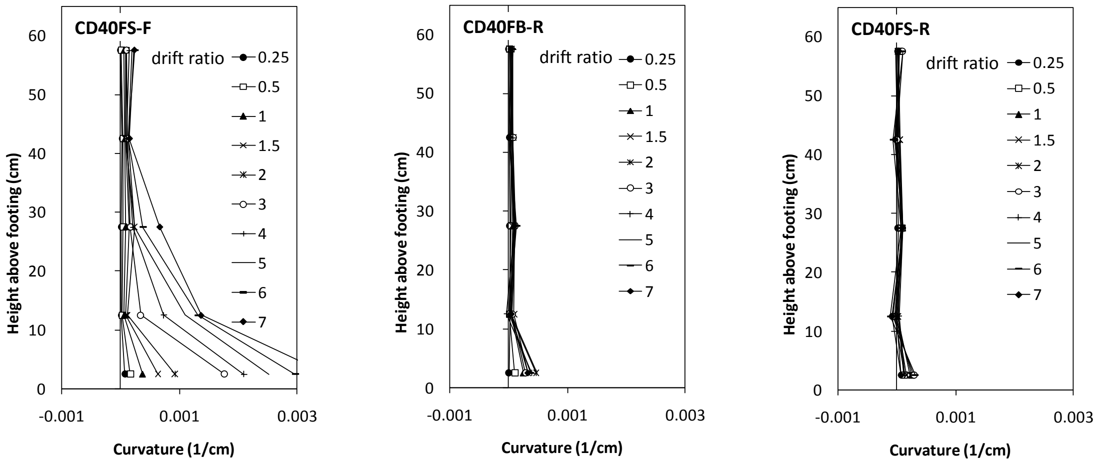

(a) CD40FS-F (b) CD40FB-R (c) CD40FS-R

Fig. 13 Curvature distributions of the cyclic loading tests of specimens CD40xx-x

(a) CD40FS-F (b) CD40FB-R (c) CD40FS-R

Fig. 14 Photographs of specimens CD40xx-x after cyclic loading tests

capacity of these columns indicated by the test results of CD40FS-F and the calculated effective yield moment from the moment–curvature curves given in Fig. 2, the moment–rotation curves for both CD40FB-R and CD40FS-R were almost linear, implying that very little plastic deformation had occurred in the columns. Similarly, the curvatures given in Fig. 13 for both CD40FB-R andCD40FS-R were much smaller than that of the fixed-base case CD40FS-F and no physical damage could be observed from photographs of these two rocking columns (Fig. 14). All these observations suggest that once the rocking moment at the footing base completely governs the response, i.e., $M_y > M_{2c}$, the plastic deformation occurring at the columns base could be very minor.

In cases with insufficient transverse reinforcements (CB40xx.x), as shown in Figs. 15–18, CB40FS-F was the benchmark test for CB40FS-R. Similarly, for the rocking case of CB40FS-R, the seismic forces that the column sustained were limited to the constant values V_{2c} and M_{2c}. Because the maximum bending moment sustained by the column was limited by value the M_{2c}, a value lower than its moment capacity at the column base indicated by CB40FS-F and the moment–curvature curve given in Fig. 2, the plastic deformation occurring in the column was minor and the corresponding moment–rotation curve shown in Fig. 16 for CB40FS-R is almost linear. The curvature distributions shown in Fig. 17 and the photographs given in Fig. 18 demonstrate a

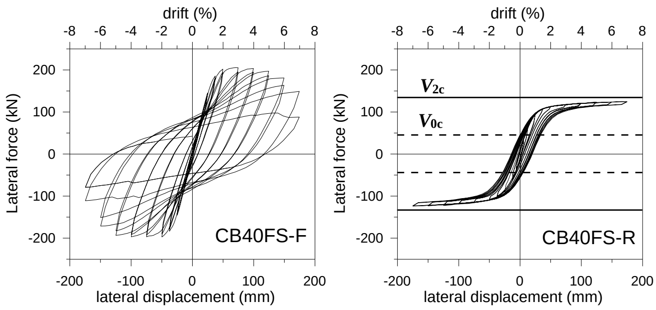

(a) CB40FS-F (b) CB40FS-R

Fig. 15 Lateral force–displacement curves of the cyclic loading tests of CB40xx-x

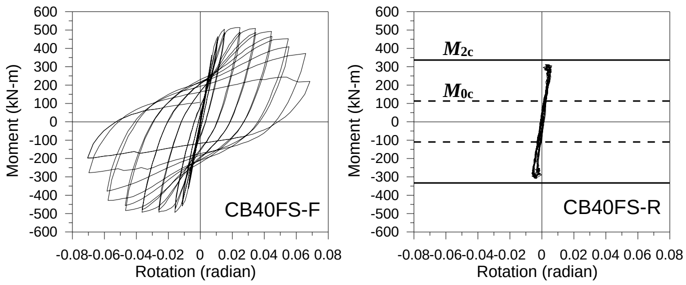

(a) CB40FS-F (b) CB40FS-R

Fig. 16 Moment–rotation curves of the cyclic loading tests of CB40xx-x

similar trend. The curvature in CB40FS-R was much smaller than that of the fixed-base case, CB40FS-F, and only minor cracks could be observed in specimen CB40FS-R, even though its transverse reinforcements were insufficient.

Another trend that can be observed from these figures is that the response behavior of the rocking base case CB40FS-R was similar to case CD40FS-R, even though the response of the corresponding fixed-base cases CB40FS-F and CD40FS-F were different. This result confirms that the ductility demand of a column can be reduced if its upper limit of the moment due to rocking is much lower than the yield moment capacity of the column base, i.e., the ratio M_y/M_{2c} is much higher than 1. For the current case, the designed ratio was M_y/M_{2c} = 1.28. This was because, in that instance, the column did not need to sustain moments with a value higher than its yield moment and would not deform into a plastic state. Thus the ductility capacity that allowed the column to deform plastically without fracture became unnecessary.

Figs. 19–22 show the experimental results for specimens with 12-D19 main reinforcements (CD30xx.x). Among these specimens, CD30FS-F was the benchmark test, representing both the fixed-base case and the case with a very large footing. Similar to the results of the CD40xx.x specimens, these results given in Fig. 19 demonstrate that, with the decrease in footing size, the nonlinear rocking behavior becomes more significant. Consequently, the plastic deformation occurring in the column base becomes minor. For instance, the moment–rotation curve for CD30FS-R shown in Fig. 20(c) is almost linear, while some plastic deformation occurred in CD30FB-R as shown in Fig. 20(b). A similar trend can also be observed in the curvature distribution plots in Fig. 21 and the photographs of the test columns in Fig. 22. This is because the calculated upper limit value of the moment M_{2c} of CD30FB-R, as shown in Fig. 20(b), was higher than the moment capacity of the column indicated by CD30FS-F in Fig. 19(a) and its design ratio of M_y/M_{2c} = 0.79 is a value much lower than 1. Therefore, before the base moment of the footing could reach its upper limit value, the column had already yielded and the moment capacity of the column governed the response behavior. On the other hand, in the case of specimen CD30FS-R, even though its design ratio of M_y/M_{2c} = 0.98 is only a little bit lower than 1, the actual moment capacity of specimen CD30FS-F, indicated in Fig. 20(a), was higher than its design value due to overstrength. This means that the actual moment capacity of CD30FB-F was higher than the maximum value of the bending moment sustained by the column, which was around 320 kNm. Thus, the column was still able to remain in an elastic state under cyclic loading.

(a) CD40FS-F (b) CD40FB-R

Fig. 17 Curvature distributions of the cyclic loading tests of specimens CB40xx-x

(a) CD40FS-F (b) CD40FB-R

Fig. 18 Photographs of the specimens CB40xx-x after cyclic loading testing

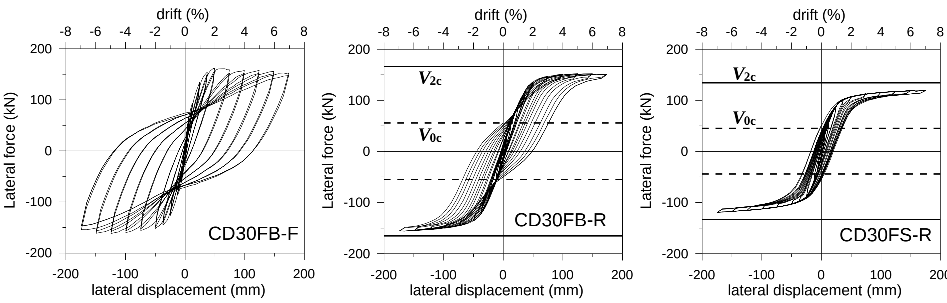

(a) CD30FS-F (b) CD30FB-R (c) CD30FS-R

Fig. 19 Lateral force–displacement curves of the cyclic loading test of CD30xx-x

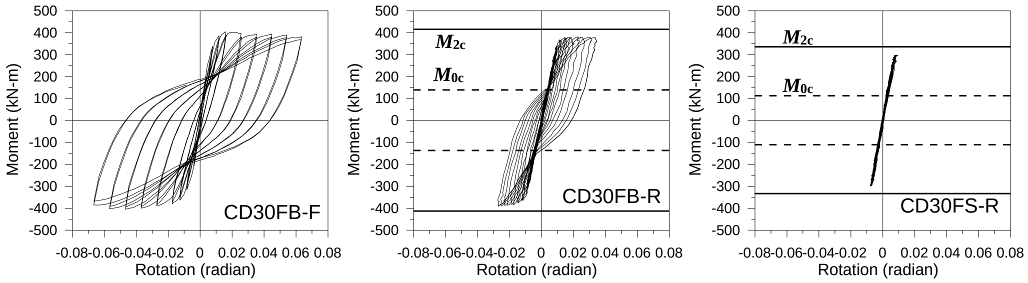

(a) CD30FS-F (b) CD30FB-R (c) CD30FS-R

Fig. 20 Moment–rotation curves of the cyclic loading test of CD30xx-x

4.4 Comparison and discussion

According to the cyclic loading test results, among those cases with a rocking base, only specimen CD30FB-R had gone through to the plastic stage. This was because it was the only specimen with an actual ratio of M_y/M_{2c} lower than 1. This result also confirms that the ratio M_y/M_{2c} is the key parameter for rocking behavior of columns with spread footing. According to the material test, the concrete compressive strength is $f_c^{'}$ = 28.5 MPa and the yield strength of the main reinforcements is F_y = 461.1MPa. Based on these test results, the effective yield moments for CD30xx.x and CD40xx.x specimens were 355.1 kNm and 466.0 kNm, respectively. Thus the actual M_y/M_{2c} ratios for CD40FS-R, CD40FB-R, CD30FS-R and CD30FB-R became 1.39, 1.12, 1.06 and 0.86, respectively. Among these specimens, only specimen CD30FB-R had a value of M_y/M_{2c} lower than 1.

The ratio M_y/M_{2c} also affected the lateral displacement due to rocking. Based on the results from the TH1 and TH2 pseudo-dynamic test, the curves of the ratio of M_y/M_{2c} versus the lateral displacements due to foundation rocking were given in Fig. 23(a), where the displacements due to rocking were obtained by multiplying the reading of the tiltmeters mounted on the footing by 3 m, the distance from the foundation base to where the lateral load was applied. Fig. 23(a) shows that cases with higher values of ratio M_y/M_{2c} had a larger lateral displacement due to rocking for the pseudo-dynamic test of TH2. However, the influence of the ratio M_y/M_{2c} on lateral displacements for the test of TH1 is not as significant as that can be observed from the test of TH2. This is because under such a minor excitation of TH1, the amount of foundation uplift for these specimens is also minor and the difference between the displacements due to rocking becomes not distinguished. Similarly, the curves of the ratio of M_y/M_{2c} versus the lateral displacements due to foundation rocking at different drift ratios for the cyclic loading test were given in Fig. 23(b), where the cases with M_y/M_{2c} = 0 represent the cases with a fixed base. For the cases with a fixed base, the lateral displacement due to foundation equals to zero. Fig. 23(b) also shows a tendency that the increase in the value of M_y/M_{2c} leads to the increase in the lateral displacement due to rocking. However, this phenomenon is more significant as M_y/M_{2c} < 1. Correspondingly, Fig. 24 shows the uplift displacements at the foundation for each specimen. By comparing the specimens with the same foundation size, it can be seen that the uplift displacements for CD30FB-R, which was the only one with a value of M_y/M_{2c} lower than 1, are obvious smaller than that of CD40FB-R. Similarly, for specimens with a smaller foundation, specimen CD40FS-R with a value of M_y/M_{2c} = 1.39 has a larger uplift displacement than that of the CD30FS-R (M_y/M_{2c} =1.06) given in Fig (d).

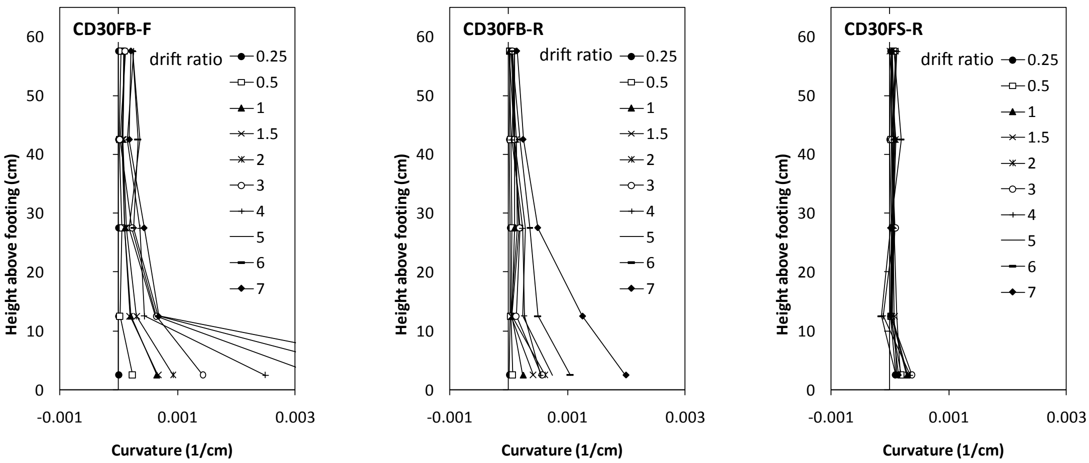

(a) CD30FS-F (b) CD30FB-R (c) CD30FS-R

Fig. 21 Curvature distributions for the cyclic loading test of specimens CD30xx-x

(a) CD40FS-F (b) CD40FB-R (c) CD40FS-R

Fig. 22 Photographs of the CD30xx-x specimens after the cyclic loading tests

To quantitatively evaluate the influence of ratio M_y/M_{2c} on the plastic deformation in the column base, the equivalent viscous damping ratios corresponding to the moment-rotation curves given in Fig. 12 and Fig. 20 were computed using Eqs. (5) and (6). This computed equivalent viscous damping ratio can be used as an indicator of the plastic deformation.

$$\zeta_{eq} = \frac{E_D}{2\pi K_{eff} \Delta_p{}^2} \tag{5}$$

$$K_{eff} = \frac{F_p - F_n}{\Delta_p - \Delta_n} \tag{6}$$

Where ζ_{eq} = equivalent viscous damping ratio; E_D = energy dissipation per cycle or area of the hysteresis loop; K_{eff} = effective stiffness; Δ_p and Δ_n = maximum positive and negative rotations of the loop, respectively; and F_p and F_n = moments at Δ_p and Δ_n, respectively.

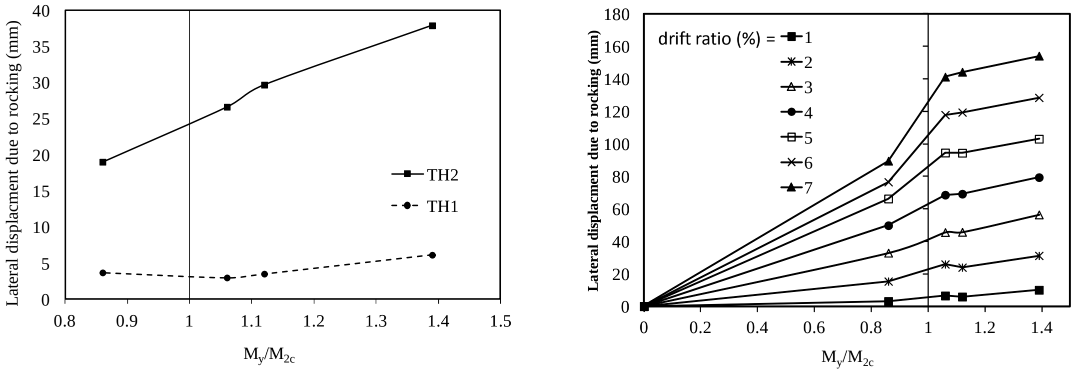

(a) Pseudo-dynamic test (b) cyclic loading test

Fig. 23 The ratio of M_y/M_{2c} versus the lateral displacement due to foundation rocking

The computed equivalent viscous damping ratios ζ_{eq} for each drift level for all the specimens were given in Fig. 25. It shows that the equivalent viscous damping ratios for the fixed base cases of CD40FS-F and CD30FB-F, which can represent cases with a value of M_y/M_{2c} = 0, were obvious larger than the other cases with a rocking base and their maximum equivalent viscous damping ratio ζ_{eq} = 27 %. Specimen CD30FB-R, which has a M_y/M_{2c} value of 0.86, had a maximum value of ζ_{eq} around 15 %. On the other hand, for the specimens with a M_y/M_{2c} value larger than 1, i.e., specimens CD40FS-R, CD40FB-R, CD30FS-R, the equivalent damping rations were all very small and their differences were not significant. This observation confirms that the extent of the decrease in plastic deformation is also dependent on the M_y/M_{2c} value. For specimens with a ratio of M_y/M_{2c} lower than 1, the plastic deformation increases with the decrease in value of M_y/M_{2c}. For specimens with a ratio of M_y/M_{2c} higher than 1, since the rocking behavior was mainly controlled by the size of the foundation and the induced plastic deformation was minor, the influence of M_y/M_{2c} on the plastic deformation was not noticeable. Correspondingly, Fig. 26 shows the average residual drift for each drift level for all the specimens. The average residual drift is the average of absolute values of drifts at zero force for each level of cyclic loading and which can also be a good indicator of the extent of the plastic deformation. This figure indicates that the specimen which has a lower value of M_y/M_{2c} has a higher residual displacement. However, as the value of M_y/M_{2c} becomes higher than 1, even though the residual displacement is still lower than cases with a value of M_y/M_{2c} lower than 1, the effect of M_y/M_{2c} become less significant. Again, this is because as M_y is larger than M_{2c}, the behavior is mainly controlled by rocking and the key factor becomes the size of footing.

The above observations further confirm that if the ratio M_y/M_{2c} is larger than 1, the response behavior of the column–footing system would be governed by rocking of the footing. On the other hand, for specimens with a M_y/M_{2c} value lower than 1 but not so low as to prevent rocking, i.e., M_y/M_{0c} >1, the uplift of the foundation becomes less significant and some plastic deformation at the column base is to be expected, as observed from the tests on specimen CD30FB-R. However, because the uplift of the foundation helps to reduce some earthquake demand, the plastic deformation at the column base did not seem to be as serious as that for the fixed-base case.

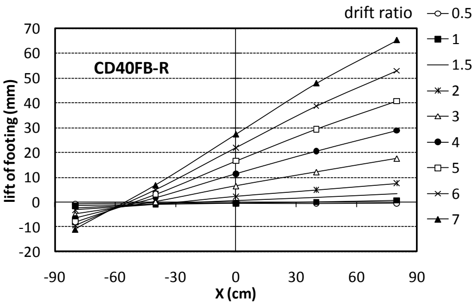

(a) CD40FB-R

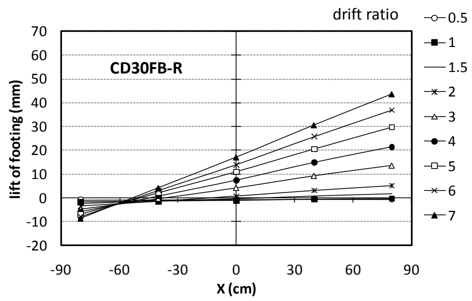

(b) CD30FB-R

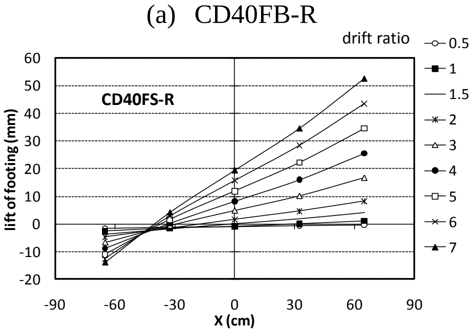

(c) CD40FS-R

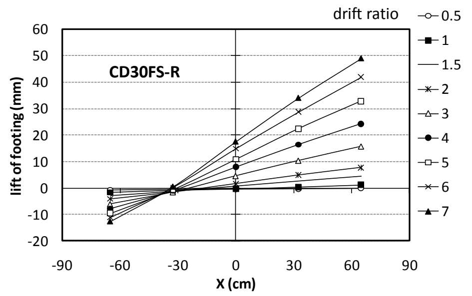

(d) CD30FS-R

Fig. 24 Uplift displacement of the foundation for the cyclic loading test

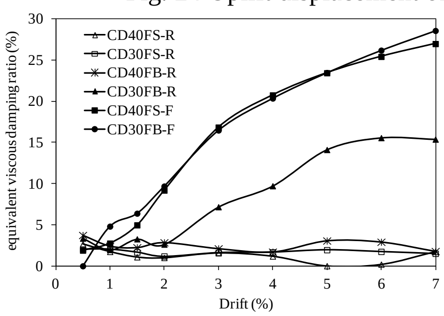

Fig. 25 Equivalent viscous damping ratios

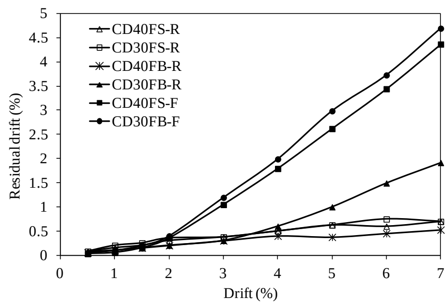

Fig. 26 Residual drifts for each drift level

5. Conclusions

In this study, a series of pseudo-dynamic and cyclic loading tests on six reinforced concrete columns with varying sizes of footing, strengths and ductility capacities were conducted. These experiments showed that the factor M_y/M_{2c}, which is the ratio of the moment capacity of the column to the moment capacity of the foundation, can be an indicator for the prediction of the rocking behavior of columns with spread footings. The cases with a higher value of ratio M_y/M_{2c} had a larger lateral displacement due to rocking under the same seismic excitation. In addition, if the footing uplift takes place, there is a decrease in the plastic deformation at the plastic hinge of the column as a result of the energy dissipation of the inelastic rocking mechanism. The extent of the decrease in plastic deformation and residual displacement is also dependent on the value of M_y/M_{2c}. For specimens with a ratio of M_y/M_{2c} higher than 1, the rocking behavior was mainly controlled by the size of the foundation. As a result, the plastic deformation would not occur at the column base and the residual displacement and the ductility demand of the column can be reduced. On the other hand, for a specimen with a M_y/M_{2c} ratio lower than 1, but not so low as to prevent the uplift of the foundation, i.e., M_y/M_{oc} >1, both rocking and column hinging can help to dissipate some energy. Therefore, its lateral displacement due to rocking would be less significant as compared to the case with a M_y/M_{2c} value higher than 1 and the plastic deformation at the column base would be less serious than a fixed-base case.

Acknowledgments

This study was funded in part by the National Science Council of Taiwan under grant number NSC 98-2625-M-492-004. The test specimens, facilities and technical support from the National Center for Research on Earthquake Engineering are also gratefully acknowledged.

References

AASHTO (2009), *Guide Specifications for LRFD Seismic Bridge Design*, (1st Edition), Washington, DC

Apostolou, M., Gazetas, G. and Garini, E. (2007), “Seismic response of slender rigid structures with foundation uplifting”, *Soil. Dyn. Earthq. Eng.*, **27,** 642-654.

Aslam, M., Goggen, W.G. and Scalise, D.T. (1980), “Earthquake rocking response of rigid bodies”, *J Struct . Div.* (ASCE), **106**(2), 377-392.

Chopra, A.K. and Yim, C.S. (1985), “Simplified earthquake analysis of structures with foundation uplift”, *J Struct. Eng.* (ASCE), **111**(4), 906-930.

Cremer, C., Pecker, A. and Davenne, L. (2001), “Cyclic macro-element for soil-structure interaction: material and geometrical non-linearities”, *Int. J. Numer. Anal. Met.*, **25** (13), 1257-1284.

Deng, L., Kutter, B.L. and Kunnath, S. (2012), “Centrifuge modeling of bridge systems designed for rocking foundations”, *J. Geotech. Geoenviron. Eng.* (ASCE). **138**(3), 225-344.

Deng, L. and Kutter, B.L. (2012), “Characterization of rocking shallow foundations using centrifuge model tests”, *Earthq. Eng. Struct. Dyn.*, **41**, 1043-1060.

Espinoza A, Mahin S (2006) Rocking of bridge piers subjected to multi-directional earthquake excitation. Fifth National Seismic Conference on Bridge & Highways, San Francisco, CA, September 18-20

FEMA (1997), *NEHRP Guidelines and Commentary for the Seismic Rehabilitation of Buildings*, Reports No. 273, Washington, D.C.

FHWA (2006), *Seismic Retrofitting Manual for Highway Structures: Part 1- Bridges*, Reports No. FHWA-HRT-05-032.

Gajan, S., Kutter, B.L., Phalen, J.D., Hutchinson, T.C. and Martin, G.R. (2005), “Centrifuge modeling of load-deformation behavior of rocking shallow foundation”, *Soil Dyn. Earthq. Eng.*, **25**, 773-783.

Gajan, S. and Kutter, B.L. (2008), “Capacity, settlement, and energy dissipation of shallow footings subjected to rocking”, *J. Geotech. and Geoenviron. Eng.* (ASCE) ,**134**(8), 1129-1141.

Gajan, S., Hutchinson, T.C., Kutter, B.L., Raychowdhury, P., Ugalde, J.A. and Stewart, J.P. (2007), *Numerical Models for Analysis and Performance-based Design of Shallow Foundations Subjected to Seismic Loading*. PEER 2007/4, Pacific Earthquake Engineering Research Center, University of California, Berkeley

Grange, S., Kotronis, P. and Mazars, J. (2009), “A macro-element to simulate 3D soil-structure interaction considering plasticity and uplift”, *Int. J. Solids Struct.*, **46**, 3651-3663.

Grange, S., Kotronis, P. and Mazars, J. (2009), “A macro-element to simulate dynamic soil-structure interaction”, *Eng. Struct.*, **31**, 3034-3046.

Grange, S., Botrugno, L., Kotronis, P. and Tamagnini, C. (2011), “The effects of soil-structure interaction on a reinforced concrete viaduct”, *Earthq. Eng. Struct. Dyn.*, **40**, 93-105.

Harden, C., Hutchinson, T.C., Kutter, B.L. and Martin, G. (2005), *Numerical Modeling of the Nonlinear Cyclic Response of Shallow Foundations*, PEER 2005/04, Pacific Earthquake Engineering Research Center, University of California, Berkeley

Housner, G.W. (1963), “The behavior of inverted pendulum structures during earthquakes”, *Bull. Seismol .Soc. Am.*, **53**(2), 403-417.

Hung, H.H., Liu, K.Y., Ho, T.H. and Chang, K.C. (2011), “An experimental study on the rocking response of bridge piers with spread footing foundations”, *Earthq. Eng. Struct. Dyn.*, **40**, 749-769.

Kawashima, K. and Nagai, T. (2006), “Effectiveness of rocking seismic isolation on bridges”, *4th International Conference on Earthquake Engineering*, Taipei, Taiwan, October 12-13.

Kelly, T.E. (2009), “Tentative seismic design guidelines for rocking structure”, *Bull. NZ Soc. Earthq. Eng.*, **42**(4), 239-274.

Kutter, B.L., Martin, G., Hutchinson, T.C., Harden, C., Gajan, S. and Phalen, J. (2005), *Workshop on Modeling of Nonlinear Cyclic Load-deformation Behavior of Shallow Foundations*, PEER 2005/14, Pacific Earthquake Engineering Research Center, University of California, Berkeley.

MOTC (2008), *Seismic Design Code for Highway Bridges*, Taiwan (in Chinese).

Palmeri, A,, Makris, N, (2008), “Response analysis of rigid structures rocking on viscoelastic foundation”, *Earthq. Eng. Struct. Dyn.*, **37**, 1039-1063.

Paolucci, R., Shirato, M. and Yilmaz, M.T. (2008), “Seismic behaviour of shallow foundations: shaking table experiments vs numerical modeling”, *Earthq. Eng. Struct. Dyn.*, **37**, 577-595.

Psycharis, I. (1982), *Dynamic Behavior of Rocking Structures Allowed to Uplift*, EERL Report 81–02, California Institute of Technology.

Sakellaraki D, Watanabe G, Kawashima K (2005) Experimental rocking response of direct foundations of bridges. Second International Conference on Urban Earthquake Engineering, Tokyo Institute of Technology, Tokyo, Japan, March 7-8, 497-504

Shirato, M., kouno, T., Asai, R., Nakani, S., Fukui, J. and Paolucci, R. (2008), “Large-scale experiments on nonlinear behavior of shallow foundations subjected to strong earthquakes”, *Soil Found.*, **48**(5), 673-692.

Taylor, P.W., Bartlett, P.E. and Wiessing, P.R. (1981), “Foundation rocking under earthquake loading”, *Proceedings of the 10th International Conference on Soil Mechanics and Foundation Engineering*, **3**, 313-322.

Tso, W.K. and Wong, C.M. (1989), “Steady state rocking response of rigid blocks, Part I: analysis”, *Earthq. Eng. Struct. Dyn.*, **18**, 89-106.

Ugalde, J.A., Kutter, B.L., Jeremić, B. and Gajan, S. (2007), “Centrifuge modeling of rocking behavior of bridges on shallow foundations”, *4th International Conference on Earthquake Geotechnical Engineering*, Thessaloniki, Greece, June 25-28.

Ugalde, J.A., Kutter, B.L. and Jeremić, B. (2010), *Rocking Response of Bridges on Shallow Foundations*, EER-2010/101, Pacific Earthquake Engineering Research Center, University of California, Berkeley

Wiessing, P.R. (1979), *Foundation Rocking on Sand*. School of Engineering Report No. 203, University of Auckland, New Zealand.

Yang, Y.B., Hung, H.H. and He, M.J. (2000), “Sliding and rocking response of rigid blocks due to horizontal excitations”, *Struct. Eng. Mech., Int. J.*, **9**(1), 1-16.

Yim, C.S., Chopra, A.K. and Panzien, J. (1980), “Rocking response of rigid blocks to earthquakes”, *Earthq. Eng. Struct. Dyn.*, **8**, 565-587.

Yim, C.S. and Chopra, A.K. (1984), “Earthquake response of structures with partial uplift on winkler foundation”, *Earthq. Eng. Struct. Dyn.*, **12**, 263-281.

Zhang, J. and Makris, N. (2001), “Rocking response of free-standing blocks under cycloidal pulses”, *J. Eng. Mech.* (ASCE), **127**(5), 473-483.

IT